AGU PUBLICATIONS

Geophysical Research Letters

RESEARCH LETTER
10.1002/2017GL072899

Key Points:
- Moderate-sized earthquakes occurred on a subsurface hidden fault
- Midcrustal earthquakes occurred as a consequence of stress perturbation by a megathrust earthquake
- The static and dynamic stress changes caused by the main shock induced aftershocks

Supporting Information:
- Supporting Information S1

Correspondence to:
T.-K. Hong,
tkhong@yonsei.ac.kr

Citation:
Hong, T.-K., J. Lee, W. Kim, I.-K. Hahm, N.-C. Woo, and S. Park (2017), The 12 September 2016 M_L5.8 midcrustal earthquake in the Korean Peninsula and its seismic implications, *Geophys. Res. Lett.*, *44*, 3131–3138, doi:10.1002/2017GL072899.

Received 31 JAN 2017
Accepted 26 MAR 2017
Accepted article online 29 MAR 2017
Published online 14 APR 2017

The 12 September 2016 M_L5.8 midcrustal earthquake in the Korean Peninsula and its seismic implications

Tae-Kyung Hong[1], Junhyung Lee[1], Woohan Kim[2], In-Kyeong Hahm[3], Nam Chil Woo[1], and Seongjun Park[1]

[1]Department of Earth System Sciences, Yonsei University, Seoul, South Korea, [2]Department of Earth and Environmental Sciences and RINS, Gyeongsang National University, Jinju, South Korea, [3]Korea Meteorological Administration, Seoul, South Korea

Abstract The seismicity in the Korean Peninsula has increased since the 2011 M_w9.0 Tohoku-Oki megathrust earthquake. Two strike-slip earthquakes with magnitudes of M_L5.1 and 5.8 occurred in the southeastern Korean Peninsula on 12 September 2016. The two events occurred within 48 min. The M_L5.8 earthquake was the largest event in the Korean Peninsula since 1978 when national seismic monitoring began. Both events produced strong high-frequency ground motions. More than 500 aftershocks with local magnitudes greater than or equal to 1.5 followed the events for 2 months. An unreported subsurface strike-slip fault with a dip of 65° to the east and a strike of N27°E was responsible for the earthquakes. The fault ruptured at depths of 11–16 km, resulting in a rupture plane of ∼26 km^2. The aftershock distribution displayed horizontal streaks at a depth of ∼14 km, which was consistent with the focal mechanism solutions from long-period waveform inversion. The number of aftershocks decreased exponentially with time. The two M_L5.1 and 5.8 earthquakes produced regional Coulomb stress changes of −4.9 to 2.5 bar. The spatial distribution of the aftershocks correlated with the Coulomb stress changes. The peak dynamic stress induced by strong ground motions reached 14.2 bar. The groundwater levels changed coseismically in some regions of decreased static stresses. The earthquakes on previously unidentified faults raised attention for the potential seismic hazards by earthquakes with long recurrence intervals.

1. Introduction

The influence of a megathrust earthquake on the long-term evolution of intraplate seismicity at regional distances remains uncertain [e.g., *Hong et al.*, 2015]. There are contradictory observations presenting both seismicity increases and decreases in stress shadows [e.g., *Jaumé and Sykes*, 1996; *Harris*, 1998; *Felzer and Brodsky*, 2005; *Mallman and Parsons*, 2008]. The Korean Peninsula is placed on a stable intraplate regime with relatively low seismicity. However, the 2011 M_w9.0 Tohoku-Oki megathurst earthquake changed the seismicity in the Korean Peninsula [*Hong et al.*, 2015]. The megathrust earthquake coseismically displaced the Korean Peninsula by 2 to 5 cm in the direction of the epicenter [*Baek et al.*, 2012; *Kim and Bae*, 2012; *Ha et al.*, 2014; *Hong et al.*, 2015; *Houng et al.*, 2016]. Postseismic displacement has occurred in the Korean Peninsula for several years since the megathrust earthquake [*Baek et al.*, 2012; *Zhou et al.*, 2012; *D. Kim et al.*, 2016].

The megathrust earthquake produced strong ground motions [*Hoshiba et al.*, 2011; *Peng et al.*, 2012] and dynamically triggered earthquakes around the peninsula for more than half a day [*Houng et al.*, 2016]. The coseismic and postseismic displacements caused temporal changes in the stress field and changed the earthquake occurrence rate as well as the frequency of large earthquakes [*Hong et al.*, 2015; *Houng et al.*, 2016]. Moderate-sized earthquakes have occurred frequently since the Tohoku-Oki earthquake. In particular, three earthquakes with magnitudes greater than or equal to M_L4.9 occurred in the Yellow Sea region between 2013 and 2014. In addition, unusual clustered earthquakes occurred at two regions in the Yellow Sea [*Hong et al.*, 2015; *Houng et al.*, 2016].

Historically, there have been many large earthquakes in the Korean Peninsula [*Lee and Yang*, 2006; *Seo et al.*, 2010; *Houng and Hong*, 2013; *Hong et al.*, 2016; *Park and Hong*, 2016]. There is growing concern that large earthquakes will occur in the near future due to the influence of the 2011 Tohoku-Oki megathrust earthquake.

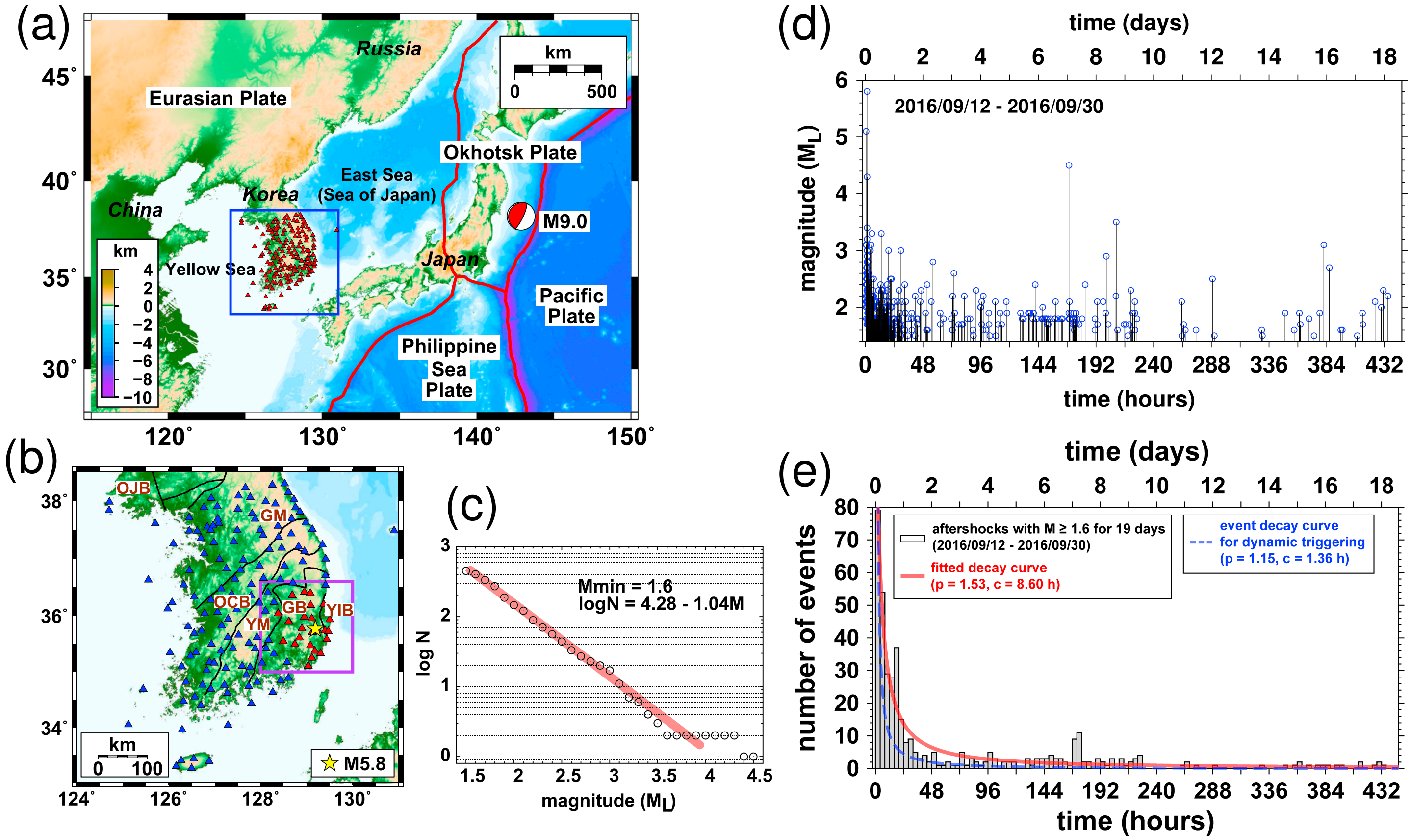

Figure 1. (a) Tectonic setting around the Korean Peninsula. The epicenter and focal mechanism solution of the 2011 M_w9.0 Tohoku-Oki earthquake are marked. (b) An enlarged map of the Korean Peninsula (rectangular region in the large map in Figure 1a) with presentation of major geological provinces. The epicenter of M_L5.8 (star) and stations (triangles) are marked. The major geological provinces are denoted: Gyeonggi massif (GM), Gyeongsang basin (GB), Okcheon belt (OCB), Ongjin basin (OJB), Yeongnam massif (YM), and Yeonil basin (YIB). (c) Determination of the Gutenberg-Richter magnitude-frequency relationship for the aftershocks. The minimum magnitude, M_{min}, ensuring the earthquake catalog completeness, is 1.6. The *b* value is 1.04. (d) Temporal distribution of magnitudes of aftershocks. (e) Temporal variation of aftershocks that follows Omori's law with parameter *p* of 1.53 and parameter *c* of 8.60 h. The earthquake occurrence rate curve (dashed line) for dynamically triggered earthquakes by the 2011 M_w9.0 megathrust earthquake is presented for comparison.

The M_L5.8 earthquake on 12 September 2016, the largest event since 1978, occurred in the southeastern Korean Peninsula. The event provides a unique opportunity to examine the properties of moderate earthquakes in the region and investigate the influence of the megathrust earthquake on regional intraplate faulting.

2. Event and Data

Two moderate-sized earthquakes with local magnitudes of M_L5.1 and 5.8 occurred within an interval of 48 min on 12 September 2016. The events occurred around the Yangsan fault zone in the southeastern Korean Peninsula that had been seismically inactive (Figure 1). The two events occurred in nearby locations. The hypocentral interevent distance is 0.90 km. The M5.8 earthquake is the largest event in the Korean Peninsula since 1978 when national seismic monitoring began. This event produced strong coseismic ground shaking, which was felt at distances of more than 300 km (Figure 2).

The two events and their aftershocks were well recorded in 160 seismic stations over the Korean Peninsula (Figure 1). The peak ground accelerations reached 4.4 m/s^2 in the E-W component, 4.2 m/s^2 in the N-S component, and 2.3 m/s^2 in vertical component at station USN at an epicentral distance of 8.2 km. Local site effects amplify the ground motions (Figure 2a). Ground motions at an epicentral distance of 8.2 km (station USN) are stronger than those at an epicentral distance of 5.8 km (station MKL). The spectra of displacement waveforms at three local stations (MKL, USN, and HDB) display characteristic high-frequency energy (Figure 2b). The responsible fault rupture was not found on the surface. We collect the information on

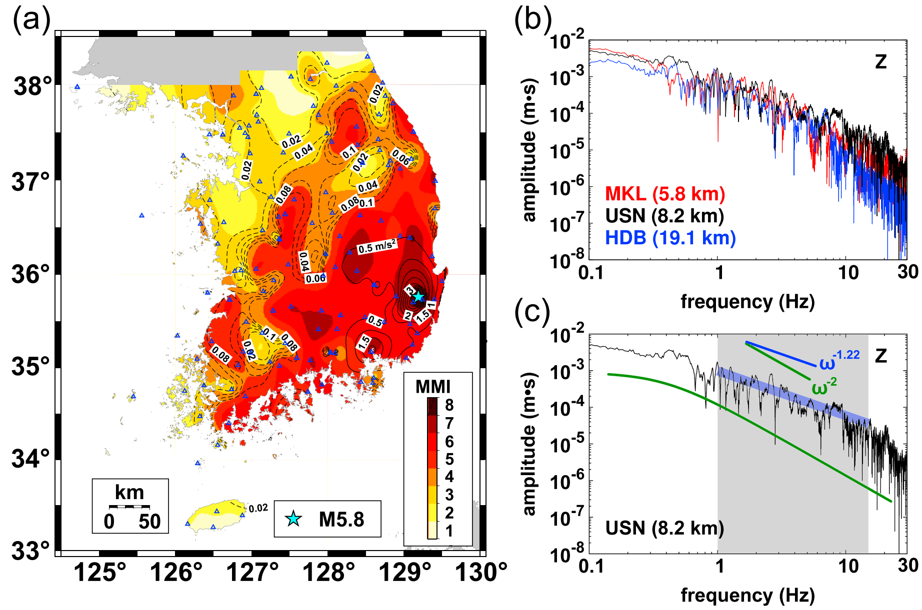

Figure 2. (a) Spatial distribution of instrumental seismic intensities in MMI scale. The peak EW directional ground accelerations are presented in contours. The peak instrumental seismic intensity is MMI 8. (b) Vertical displacement spectra at stations MKL, USN, and HDB. The epicentral distances are noted. (c) Estimation of frequency-dependent decay rate of displacement spectra in a frequency range of 1–15 Hz, presenting $\omega^{-1.22(\pm 0.02)}$, where ω is the frequency. A theoretical displacement spectra with the corner frequency of 0.39 Hz for an arbitrary seismic moment is presented for comparison (blue solid line). Strong high-frequency energy is observed.

groundwater levels from 210 national groundwater monitoring stations that are installed at depths of ~70 m beneath the surface. The sampling rate of groundwater level is one sample for every hour.

We analyze 128 earthquakes with magnitudes of M_L1.95–5.80 from 12 September 2016 to 2 October 2016. The largest aftershock, with a magnitude of M_L4.5, occurred 7 days after the main shock. The number of aftershocks with magnitudes greater than 1.5 is 521 as of 17 November 2016. The magnitudes and numbers of aftershocks generally decreased with time (Figure 1). The focal depths range between 11 and 16 km. Most events are distributed at depths between 13 and 15 km (see supporting information).

3. Methods and Process

We perform a long-period waveform inversion [*Dreger and Helmberger*, 1990; *Hong et al.*, 2015] based on a global-averaged one-dimensional (1-D) velocity model [*Kennett et al.*, 1995] to determine the focal mechanism solutions of the earthquakes. We determine a set of hypocentral parameters generating the best fit synthetic waveforms [*Saikia*, 1994]. The focal mechanism solutions of the M_L5.1 and M_L5.8 earthquakes and several moderate-size aftershocks are determined based on three to five seismic records with epicentral distances of 105.4 km to 354.5 km (Figure 3). The frequency band is 0.05 to 0.12 Hz, which is slightly adjusted depending on the waveforms (see supporting information).

We refine the hypocentral parameters of the events using a velocity-searching hypocentral inversion method (VELHYPO) that is particularly effective for hypocentral-parameter inversion for earthquakes in heterogeneous media, such as fault zones [*Kim et al.*, 2014; *W. Kim et al.*, 2016]). The hypocentral-parameter inversion method is based on *P* and *S* arrival times that were manually picked from three-component waveforms. We analyze 11 to 25 three-component waveforms for each event to determine the hypocentral parameters (Figure 1). We estimated the *P* arrival times from 2691 three-component waveforms and the *S* arrivals from 473 three-component waveforms.

The dense azimuthal coverage of stations and effective hypocentral-parameter inversion method allow us to determine the hypocentral parameters with high accuracy *Kim et al.*, 2014; *W. Kim et al.*, 2016]. The *P* traveltime residuals range between −0.198 and 0.135 s. The average is 7.47×10^{-7} s, and the standard deviation is 0.032 s. The *S* traveltime residuals range between −0.300 and 0.402 s. The average is −0.051 s, and the standard

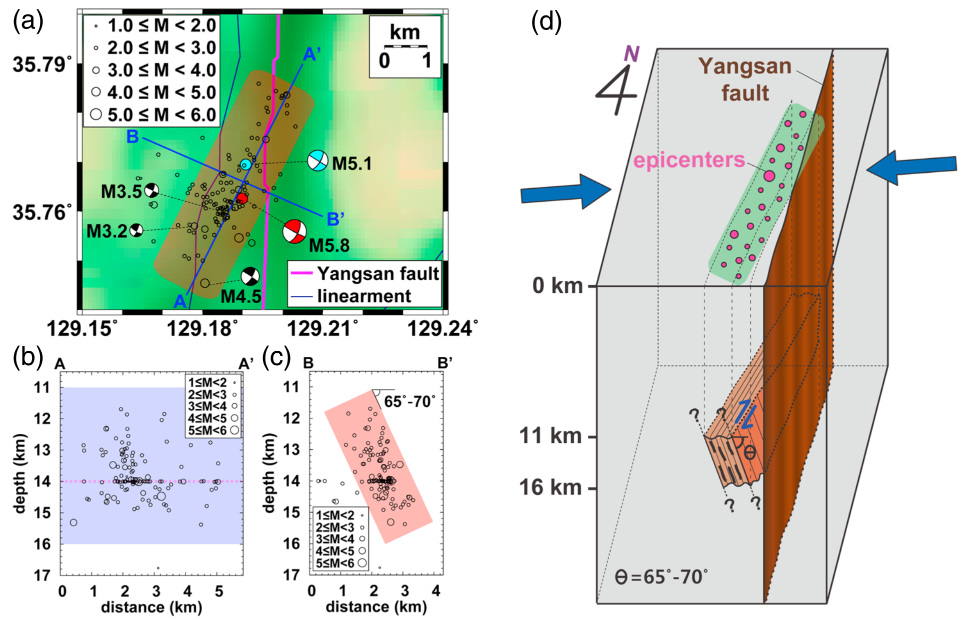

Figure 3. (a) Map view of epicenters of the main shock and aftershocks. Focal mechanism solutions from long-period waveform inversion are presented. Vertical event distribution along cross sections (b) AA′ and (c) BB′. The vertical event distribution along BB′ illuminates the fault dip angle of 65°–70°. (d) A schematic model of the responsible fault and relationship to Yangsan fault. An ENE-WSW directional compressional stress field marked with arrows is applied in the region.

deviation is 0.084 s. The horizontal and vertical location errors in 95% confidence level were less than 27 m and 50 m, respectively. The traveltime and location errors are small enough to certify the accuracy of the inversion.

VELHYPO yields a velocity model for every hypocentral-parameter inversion (Figure 3). The inverted velocity models are consistent with each other, supporting a stable inversion (see supporting information). In addition, the average velocity model agrees with regional studies [e.g., *Chang and Baag*, 2006]. We calculate the station correction terms from the traveltime residuals. The station correction terms present characteristic regional variations that increase with epicentral distance (see supporting information). The observation suggests a lateral perturbation of crustal structure in the region.

The frequency contents of radiated energy are examined by comparing between the observed and theoretical displacement waveform spectra [*Brune*, 1970]. The corner frequency of displacement spectrum is determined from an empirical relationship between the seismic moment and corner frequency [*Xie*, 2002; *Hong*, 2010] (see supporting information for the details). We examine the high-frequency decay rate of displacement spectra in a frequency range of 1–15 Hz.

The aftershock occurrence rates decay following a modified Omori's law [*Utsu and Ogata*, 1995]:

$$r(t) = \frac{K}{(t+c)^p}, \tag{1}$$

where $r(t)$ is the number of aftershocks per unit time, and t is the lapsed time in hours after the main shock. We determine a set of unknowns K, c, and p that maximizes a log likelihood function. We estimate the seismic intensity in the modified Mercalli intensity (MMI) scale from seismic waveforms [*Park and Hong*, 2014]

$$I = 3.11 \log \bar{S} + 10.61, \tag{2}$$

where $\bar{S}$ is the log-averaged horizontal acceleration spectral amplitude with units of m/s in the frequency band of 4 – 10 Hz.

We calculate the Coulomb stress change, ΔCFS that is induced by the earthquakes [e.g., *Harris*, 1998]:

$$\Delta \text{CFS} = \Delta\tau - \mu(\Delta\sigma_n - \Delta p), \tag{3}$$

where $\Delta\tau$ is the shear stress change, μ is the frictional coefficient, $\Delta\sigma_n$ is the normal stress changes (positive for increased compression), and Δp is the pore fluid pressure change. We simplify the expression to be [*King et al.*, 1994; *Toda et al.*, 2005]

$$\Delta\text{CFS} = \Delta\tau - \mu' \, \Delta\sigma_n, \tag{4}$$

where μ' is the effective frictional coefficient. The effective frictional coefficient μ' is set at 0.4 [*Nalbant et al.*, 1998; *Ma et al.*, 2005; *Toda et al.*, 2005; *Freed et al.*, 2007; *Catalli and Chan*, 2012; *Hong et al.*, 2015]. We assume the fault dimension using an empirical relationship based on the seismic moment [*Wells and Coppersmith*, 1994]. The Coulomb stress change is calculated for optimally oriented strike-slip faults. The ambient regional stress field is assumed to be N75°E directional compression with a strength of 65 bars [*Junn et al.*, 2002; *Choi et al.*, 2012; *Hong et al.*, 2015]. We set the lithospheric Young's modulus to be 80 GPa, and the Poisson's ratio to be 0.25 [*King et al.*, 1994; *Toda et al.*, 2005; *Hong et al.*, 2015].

The peak dynamic stress, σ_d, induced by a ground motion is given by

$$\sigma_d = \gamma_s \frac{\dot{u}_d}{v_s}, \tag{5}$$

where γ_s is the shear modulus, $\dot{u}_d$ is the peak ground velocity (PGV), and v_s is the shear wave velocity. We set the shear wave velocity (v_s) to be 3.58 km/s and the shear modulus (γ_s) to be 34.95 GPa, considering the seismic properties at a depth of 10 km in the crust of the Korean Peninsula [*Houng et al.*, 2016]. The peak dynamic stress changes are calculated based on the seismic waveforms from the seismic stations that were deployed uniformly in the Korean Peninsula.

4. Results

The instrumental seismic intensity at the epicenter is MMI 8. The peak instrumental seismic intensity reached MMI 7 in the northwestern Gyeongsang basin, which is located several tens of kilometers away from the epicenter (Figure 2a). The region of peak seismic intensity coincides with the region of crustal seismic amplification [*Hong and Lee*, 2012; *Jo and Hong*, 2013]. The region of MMI 6 expands up to a distance of more than 100 km from the epicenter. The seismic intensity decays slowly with distance in the Precambrian massif blocks.

The seismic waveforms of the main shock are rich with high-frequency energy (Figure 2b). The displacement spectra display an apparent decay rate of $\omega^{-1.2(\pm 0.02)}$ in a frequency band of 1–15 Hz where ω is the frequency. The apparent decay rate is much smaller than the expected decay rate of ω^{-2} (Figure 2c; see supporting information) [*Brune*, 1970]. The high-frequency signals may indicate energy radiation from small-scale heterogeneities, which suggests a rupture on a fresh and rough fault plane. The high-frequency energy decays fast with distance (Figure 2b).

The minimum magnitude of the aftershock catalog is M_L1.6 (Figure 1c). The b value of the Gutenberg-Richter magnitude-frequency relationship for aftershocks is 1.04. Parameter p in equation (1) is determined to be 1.53, and parameter c is given by 8.60 h (Figure 1e). It is noteworthy that the parameters p and c for dynamically triggered earthquakes in the Korean Peninsula by the 2011 M_w9.0 Tohoku-Oki megathrust earthquake were determined by 1.15 and 1.36 h, respectively [*Houng et al.*, 2016]. The aftershock occurrence rate decays more slowly than the dynamically triggered earthquake occurrence rate (Figure 1e). The observation suggests that the static-stress change may be more effective for earthquake triggering in a stable intraplate region than the dynamic stress change.

The focal mechanism solution of the M_L5.8 event from a long-period waveform inversion suggests a N27°E directional fault. The dip is 65°. The moment magnitude is M_w5.4. The focal mechanism solution of M_L5.1 event suggests a strike of N32°E and a dip of 70°. The moment magnitude is M_w5.0. The distribution of aftershocks agrees with the fault geometry. The focal mechanism solutions of moderate-size aftershocks present a similar fault geometry.

The focal depths of earthquakes range between 11 and 16 km (Figure 3). The focal depth distribution of aftershock displays an eastward dipping, which agrees with the fault dipping geometry of the M_L5.8 and M_L5.1 events. The clustered events suggests the dimension of the fault plane to be ~26 km^2. The earthquakes are concentrated laterally at a depth of 14 km. The spatial distribution of aftershocks is consistent with the fault

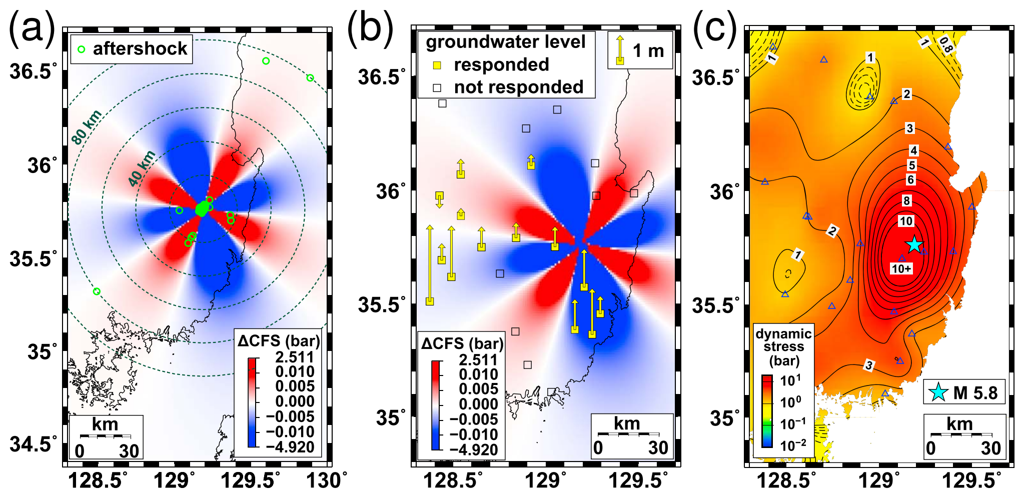

Figure 4. (a) Spatial distribution of aftershocks over the Coulomb stress changes induced by the M_L 5.1 and 5.8 earthquakes. The aftershocks occurred in the regions of increased Coulomb stress changes. (b) Spatial distribution of groundwater level changes for 3 days after the main shock. The groundwater levels are rarely correlated with the Coulomb stress changes. (c) Peak dynamic stress induced by seismic waves from the M_L 5.8 earthquake. The seismic stations are marked with triangles. Groundwater level changes are reasonably correlated with the dynamic stress changes.

geometry inferred from the focal mechanism solutions. The focal mechanism solutions and the spatial distribution of events suggest that the events occurred on a fault oriented at a small angle with respect to the Yangsan fault (Figure 3).

The M_L 5.1 and M_L 5.8 earthquakes lowered the Coulomb stress in the fault region and increased the Coulomb stress in the regions off the fault along the directions of fault strike (NNE and SSW) and axis normal (WNW-ESE) (Figure 4a). Also, the Coulomb stresses were lowered in the intervening regions. The Coulomb stress changes range between −4.9 and 2.5 bar. The strong seismic waves induced the peak dynamic stress changes greater than 10 bar around the epicenter (Figure 4c). Large peak dynamic stress changes were observed along the direction of fault strike. The Coulomb stress changes at the locations of three local stations (USN, MKL, and HDB) are 0.22, 0.15, and 0.05 bar. On the other hand, the peak dynamic stress changes at the same locations are 14.2, 9.90, and 5.03 bar. The peak dynamic stress changes are 60 to 100 times larger than the Coulomb stress changes.

Most aftershocks occurred around the fault where large dynamic stresses were induced. The remote postseismicity is scattered over the regions of elevated static stresses, displaying spatial correlation between the Coulomb stress changes and postseismicity (Figure 4a; see also the supporting information). Some postseismic events occurred around the paleo-rifting region in the East Sea where a weak static-stress increase was observed [*Choi et al.*, 2012; *Hong and Choi*, 2012].

The high postseismicity in the near field may be a consequence of medium response to large dynamic stress changes [e.g., *Kilb et al.*, 2000; *Belardinelli et al.*, 2003]. The postseismicity in remote regions may be associated with the elevated static stress by the main shock. The remotely triggered earthquakes occurred in regions with Coulomb stress increases less than 0.01 bar [e.g., *King et al.*, 1994; *Toda et al.*, 2012; *Convertito et al.*, 2016].

We also observed coseismic groundwater level changes in the south and west regions from the epicenter where the Coulomb stress decreased (Figure 4b). The groundwater level changes appear to be hardly dependent on the distance.

5. Discussion and Conclusions

We investigated the properties of the 12 September 2016 M_L 5.1 and 5.8 earthquakes and their aftershocks. The events occurred in a buried strike-slip fault striking N27°E at depths of 11–16 km. The dimension of fault plane is ~26 km^2. The fault plane dips to the east with an angle of 65°. The focal mechanism solutions of events are consistent with the spatial distribution of the aftershocks. The responsible fault laid across the Yangsan fault. High-frequency energy is rich in the seismic waveforms, suggesting a rupture of rough or fresh fault plane.

The number of aftershocks decreased with time exponentially following the Omori law. The M_L5.1 and 5.8 events increased the Coulomb stresses on the regions in the directions of the fault strike and axis normal. The Coulomb stress decreased on the fault region. The peak dynamic stress changes were 60 to 100 times larger than the Coulomb stress changes around the epicenter. Most near-field aftershocks occurred on the fault region of large dynamic stress changes. On the other hand, the remotely induced aftershocks occurred in the regions of elevated Coulomb stresses. The spatial distribution of postseismicity suggests that both the dynamic and static-stress changes affect the postseismicity. Also, the medium properties and tectonic structures may play additional roles in inducing postseismicity.

Large groundwater level changes were observed in some regions of decreased Coulomb stresses. The complex variation of groundwater level changes may be a result of spatial heterogeneity in poroelastic properties and effectiveness of shallow-layer compaction that are dependent on the local geology, bedrock condition, rock compression, aquifer composition, and stream discharge [e.g., *Roeloffs*, 1998; *Manga et al.*, 2012; *Shi et al.*, 2014; *Nespoli et al.*, 2016].

The absence of a surface rupture despite the moderate-sized earthquakes may suggest the possible presence of hidden faults responsible for large historical earthquakes [*Houng and Hong*, 2013]. The ambient stress field in the crust was changed by the 2011 Tohoku-Oki megathrust earthquake, causing an increase of the earthquake occurrence rate [*Hong et al.*, 2015]. The seismicity increase and stress induction by the 2011 Tohoku-Oki megathrust earthquake and the 12 September 2016 M_L5.8 earthquake may increase the possibility of large events in the near future [e.g., *King et al.*, 1994; *Felzer and Brodsky*, 2005]. It may be desirable to investigate the subsurface faults to mitigate the potential seismic hazards.

Acknowledgments
We are grateful to Jeroen Ritsema (editor) and two anonymous reviewers for valuable review comments. The seismic waveform data analyzed in this study were collected from the website of the Korea Meteorological Administration (KMA, http://www.kma.go.kr), which is open to the public. This work was supported by the Korea Meteorological Administration Research and Development Program under grant KMIPA 2015-7040. In addition, this research was partly supported by the Basic Science Research Program through the National Research Foundation of Korea (NRF) funded by the Ministry of Education (NRF-2015R1D1A1A01060198).

References

Baek, J., Y. H. Shin, S. H. Na, N. V. Shestakov, P. H. Park, and S. Cho (2012), Coseismic and postseismic crustal deformations of the Korean Peninsula caused by the 2011 M_W 9.0 Tohoku earthquake, Japan, from Global Positioning System data, *Terra Nova*, *24*, 295–300.

Belardinelli, M. E., A. Bizzarri, and M. Cocco (2003), Earthquake triggering by static and dynamic stress changes, *J. Geophys. Res.*, *108*, 2135, doi:10.1029/2002JB001779.

Brune, J. (1970), Tectonic stress and the spectra of seismic shear waves from earthquakes, *J. Geophys. Res.*, *75*, 4997–5009.

Catalli, F., and C. H. Chan (2012), New insights into the application of the Coulomb model in real-time, *Geophys. J. Int.*, *188*, 583–599.

Chang, S.-J., and C.-E. Baag (2006), Crustal structure in Southern Korea from joint analysis of regional broadband waveforms and travel times, *Bull. Seismol. Soc. Am.*, *96*, 856–870.

Choi, H., T.-K. Hong, X. He, and C.-E. Baag (2012), Seismic evidence for reverse activation of a paleo-rifting system in the East Sea (Sea of Japan), *Tectonophysics*, *572–573*, 123–133.

Convertito, V., R. De Matteis, and A. Emolo (2016), Investigating triggering of the aftershocks of the 2014 Napa earthquake, *Bull. Seismol. Soc. Am.*, *106*, 2063–2070.

Dreger, D. S., and D. V. Helmberger (1990), Broadband modeling of local earthquakes, *Bull. Seismol. Soc. Am.*, *80*, 1162–1179.

Felzer, K. R., and E. E. Brodsky (2005), Testing the stress shadow hypothesis, *J. Geophys. Res.*, *110*, B05S09, doi:10.1029/2004JB003277.

Freed, A. M., S. T. Ali, and R. Bürgmann (2007), Evolution of stress in Southern California for the past 200 years from coseismic, postseismic and interseismic stress changes, *Geophys. J. Int.*, *169*, 1164–1179.

Ha, J., K. D. Park, J. Won, and M. B. Heo (2014), Investigations into co-seismic deformation and strain in South Korea following the 2011 Tohoku-Oki earthquake using GPS CORS data, *KSCE J. Civ. Eng.*, *18*, 634–638.

Harris, R. A. (1998), Introduction to special section: Stress triggers, stress shadows, and implications for seismic hazard, *J. Geophys. Res.*, *103*(B10), 24347–24358.

Hong, T.-K. (2010), *Lg* attenuation in a region with both continental and oceanic environments, *Bull. Seismol. Soc. Am.*, *100*(2), 851–858.

Hong, T.-K., and H. Choi (2012), Seismological constraints on the collision belt between the North and South China blocks in the Yellow Sea, *Tectonophysics*, *570–571*, 102–113.

Hong, T. K., and K. Lee (2012), $M_b(Pn)$ Scale for the Korean Peninsula and site-dependent *Pn* amplification, *Pure Appl. Geophys.*, *169*, 1963–1975.

Hong, T. K., J. Lee, and S. E. Houng (2015), Long-term evolution of intraplate seismicity in stress shadows after a megathrust, *Phys. Earth Planet. Inter.*, *245*, 59–70.

Hong, T. K., S. Park, and S. E. Houng (2016), Seismotectonic properties and zonation of the far-eastern Eurasian plate around the Korean Peninsula, *Pure Appl. Geophys.*, *173*, 1175–1195.

Hoshiba, M., K. Iwakiri, N. Hayashimoto, T. Shimoyama, K. Hirano, Y. Yamada, Y. Ishigaki, and H. Kikuta (2011), Outline of the 2011 off the Pacific coast of Tohoku earthquake (M_w 9.0)-earthquake early warning and observed seismic intensity, *Earth Planets Space*, *63*, 547–551.

Houng, S. E., and T. K. Hong (2013), Probabilistic analysis of the Korean historical earthquake records, *Bull. Seismol. Soc. Am.*, *103*, 2782–2796.

Houng, S. E., J. Lee, and T. K. Hong (2016), Dynamic seismic response of a stable intraplate region to a megathrust earthquake, *Tectonophysics*, *689*, 67–78.

Jaumé, S. C., and L. R. Sykes (1996), Evolution of moderate seismicity in the San Francisco Bay region, 1850 to 1993: Seismicity changes related to the occurrence of large and great earthquakes, *J. Geophys. Res.*, *101*(B1), 765–789.

Jo, E., and T. K. Hong (2013), V_P/V_S ratios in the upper crust of the southern Korean Peninsula and their correlations with seismic and geophysical properties, *J. Asian Earth Sci.*, *66*, 204–214.

Junn, J.-G., N.-D. Jo, and C.-E. Baag (2002), Stochastic prediction of ground motions in southern Korea, *Geosci. J.*, *6*(3), 203–214.

Kennett, B. L. N., E. R. Engdahl, and R. Buland (1995), Constraints on seismic velocities in the Earth from traveltimes, *Geophys. J. Int.*, *122*, 108–124.

Kilb, D., J. Gomberg, and P. Bodin (2000), Triggering of earthquake aftershocks by dynamic stresses, *Nature*, *408*(6812), 570–574.

Kim, D., K. D. Park, J. Ha, D. H. Sohn, and J. Won (2016), Geodetic analysis of post-seismic crustal deformations occurring in South Korea due to the Tohoku-Oki earthquake, *KSCE J. Civ. Eng.*, *20*(7), 2885–2892.

Kim, S. K., and T. S. Bae (2012), Analysis of crustal deformation on the Korea Peninsula after the 2011 Tohoku earthquake, *J. Korean Soc. Surv. Geod. Photogramm. Cartography*, *30*, 87–96.

Kim, W., T.-K. Hong, and T.-S. Kang (2014), Hypocentral parameter inversion for regions with poorly known velocity structures, *Tectonophysics*, *627*, 182–192.

Kim, W., T. K. Hong, J. Lee, and T. A. Taira (2016), Seismicity and fault geometry of the San Andreas fault around Parkfield, California and their implications, *Tectonophysics*, *677*, 34–44.

King, G. C. P., R. S. Stein, and J. Lin (1994), Static stress changes and the triggering of earthquakes, *Bull. Seismol. Soc. Am.*, *84*(3), 935–953.

Lee, K., and W. S. Yang (2006), Historical seismicity of Korea, *Bull. Seismol. Soc. Am.*, *96*, 846–855.

Ma, K. F., C. H. Chan, and R. S. Stein (2005), Response of seismicity to Coulomb stress triggers and shadows of the 1999 $M_w=7.6$ Chi-Chi, Taiwan, earthquake, *J. Geophys. Res.*, *110*, B05S19, doi:10.1029/2004JB003389.

Mallman, E. P., and T. Parsons (2008), A global search for stress shadows, *J. Geophys. Res.*, *113*, B12304, doi:10.1029/2007JB005336.

Manga, M., I. Beresnev, E. E. Brodsky, J. E. Elkhoury, D. Elsworth, S. Ingebritsen, D. C. Mays, and C. Y. Wang (2012), Changes in permeability by transient stresses: Field observations, experiments and mechanisms, *Rev. Geophys.*, *50*, RG2004, doi:10.1029/2011RG000382.

Nalbant, S. S., A. Hubert, and G. C. King (1998), Stress coupling between earthquakes in northwest Turkey and the north Aegean Sea, *J. Geophys. Res.*, *103*, 24469–24486.

Nespoli, M., M. Todesco, E. Serpelloni, M. E. Belardinelli, M. Bonafede, M. Marcaccio, A. P. Rinaldi, L. Anderlini, and A. Gualandi (2016), Modeling earthquake effects on groundwater levels: Evidences from the 2012 Emilia earthquake (Italy), *Geofluids*, *16*(3), 452–463.

Park, S., and T. K. Hong (2014), Joint determination of event location and magnitude from historical seismic damage records, *Eos Trans, AGU*, *91*(26), Meet. Am. Suppl., Abstract S11A-4332.

Park, S., and T. K. Hong (2016), Joint determination of event epicenter and magnitude from seismic intensities, *Bull. Seismol. Soc. Am.*, *106*, 499–511.

Peng, Z., C. Aiken, D. Kilb, D. R. Shelly, and B. Enescu (2012), Listening to the 2011 magnitude 9.0 Tohoku-Oki, Japan, earthquake, *Seismol. Res. Lett.*, *83*, 287–293.

Roeloffs, E. A. (1998), Persistent water level changes in a well near Parkfield, California, due to local and distant earthquakes, *J. Geophys. Res.*, *103*, 869–889.

Saikia, C. K. (1994), Modified frequency-wavenumber algorithm for regional seismograms using Filon's quadrature: Modelling of Lg waves in eastern North America, *Geophys. J. Int.*, *118*, 142–158.

Seo, J. M., I. K. Choi, and H. M. Rhee (2010), A study of the historical earthquake catalog and Gutenberg-Richter parameter values of the Korean Peninsula, *Nucl. Eng. Technol.*, *42*, 55–64.

Shi, Z., G. Wang, C. Y. Wang, M. Manga, and C. Liu (2014), Comparison of hydrological responses to the Wenchuan and Lushan earthquakes, *Earth Planet. Sci. Lett.*, *391*, 193–200.

Toda, S., R. S. Stein, K. Richards-Dinger, and S. B. Bozkurt (2005), Forecasting the evolution of seismicity in Southern California: Animations built on earthquake stress transfer, *J. Geophys. Res.*, *110*, B05S16, doi:10.1029/2004JB003415.

Toda, S., R. S. Stein, G. C. Beroza, and D. Marsan (2012), Aftershocks halted by static stress shadows, *Nat. Geosci.*, *5*, 410–413.

Utsu, T., and Y. Ogata (1995), The centenary of the Omori formula for a decay law of aftershock activity, *J. Phys. Earth*, *43*, 1–33.

Wells, D. L., and K. J. Coppersmith (1994), New empirical relationships among magnitude, rupture length, rupture width, rupture area, and surface displacement, *Bull. Seismol. Soc. Am.*, *84*, 974–1002.

Xie, J. (2002), Source scaling of Pn and Lg spectra and their ratios from explosions in central Asia: Implications for the identification of small seismic events at regional distances, *J. Geophys. Res.*, *107*(B7), 2128, doi:10.1029/2001JB000509.

Zhou, X., W. Sun, B. Zhao, G. Fu, J. Dong, and Z. Nie (2012), Geodetic observations detecting coseismic displacements and gravity changes caused by the $M_w = 9.0$ Tohoku-Oki earthquake, *J. Geophys. Res.*, *117*, B05408, doi:10.1029/2011JB008849.